Leader-laggard relationship of chaos synchronization in mutually coupled vertical-cavity surface-emitting lasers with time delay

Mitsutoshi Ozaki,[1] Hiroyuki Someya,[1] Takaya Mihara,[1] Atsushi Uchida,[1,2] Shigeru Yoshimori,[1]
Krassimir Panajotov,[3] and Marc Sciamanna[4]
[1]*Department of Electronics and Computer Systems, Takushoku University, 815-1 Tatemachi, Hachioji, Tokyo 193-0985, Japan*
[2]*Department of Information and Computer Sciences, Saitama University, 255 Shimo-Okubo, Sakura-ku, Saitama city, Saitama, 338-8570, Japan*
[3]*Department of Applied Physics and Photonics (IR-TONA), Vrije Universiteit Brussel, Pleinlaan 2, B-1050 Brussels, Belgium*
[4]*Supélec, Laboratoire Matériaux Optiques, Photonique et Systèmes (LMOPS), CNRS UMR-7132, Unité de Recherche Commune Supélec et Université de Metz, 2 Rue Edouard Belin, F-57070 Metz, France*
(Received 21 June 2008; revised manuscript received 8 December 2008; published 13 February 2009)

We experimentally and numerically observe synchronization of chaos in two mutually coupled vertical-cavity surface-emitting lasers (VCSELs) with time delay. We observe in-phase and antiphase synchronization of polarization-resolved chaotic temporal wave forms under the condition of wavelength matching. We investigate leader-laggard relationship between two chaotic wave forms of mutually coupled VCSELs and find that the laser with longer wavelength becomes the leader.

DOI: 10.1103/PhysRevE.79.026210 PACS number(s): 05.45.Xt, 42.65.Sf, 42.55.Px

I. INTRODUCTION

Vertical-cavity surface-emitting lasers (VCSELs) have been considered as devices for optical communications and wireless local area networks. These semiconductor lasers emit light in direction perpendicular to the surface of the active region and therefore, have some advantages compared to conventional edge-emitting lasers: low threshold current, compact, high efficiency, large modulation bandwidth, and wafer-scale integration capability for large array configuration. Because of their short cavity length (a few micron) VCSELs emit in a single-longitudinal mode. VCSELs are very sensitive to optical injection or optical feedback due to their short cavity length, in spite of the high reflectivity of their facets.

The polarization dynamics of VCSELs have been intensively investigated for many years [1–7]. Specific polarization mode hopping and polarization switching features that accompany VCSEL nonlinear dynamics have also been reported recently [5–7]. Chaotic VCSELs have attracted increasing interest for applications in chaotic secure communications in optical local area networks: Data are encrypted into a chaotic carrier emitted by a transmitter laser and then recovered thanks to the chaos synchronization properties of a receiver laser. Synchronization of chaos in unidirectionally coupled VCSELs has been studied numerically [8]. Experimental observation of chaos synchronization in VCSELs has been reported in mutual [9] and unidirectional [10] coupling configurations. A signal transmission embedded on chaotic wave forms in VCSELs has been demonstrated experimentally [11]. However, the detailed characteristics of chaos synchronization in coupled VCSELs have not been well understood yet. For example, symmetry breaking and leader-laggard relationship have been observed in mutually coupled edge-emitting semiconductor lasers [12–14] and fiber lasers [15], but not in VCSELs. The polarization dynamics may play a crucial role for the synchronization characteristics in coupled VCSELs.

In this study, we experimentally observe synchronization of chaos in two mutually coupled VCSELs. We observe in-phase and antiphase synchronization of polarization-resolved chaotic temporal wave forms under the condition of wavelength matching. We also investigate leader-laggard relationship between two chaotic wave forms of coupled VCSELs and find the condition where one of the two lasers becomes the leader or the laggard.

II. VCSEL CHARACTERISTICS

We use two single-transverse-mode VCSELs (Fuji Xerox Inc., AS-0001-K) in our experiment. First, we measure the light-versus-current (L-I) characteristics of the two solitary VCSELs (called VCSEL 1 and VCSEL 2). The polarization modes are resolved into two orthogonal components (x mode and y mode) by using a polarizer. Here we define x mode as the first lasing polarization mode after the lasing threshold. We measure the light power for x mode, y mode, and the total intensity as a function of the injection current for VCSEL 1 and 2, as shown in Figs. 1(a) and 1(b), respectively. The lasing thresholds are $I_{th,1}=0.39$ mA and $I_{th,2}=0.37$ mA for VCSEL 1 and 2, respectively. One polarization mode (x mode) starts lasing just above the threshold. For VCSEL 1, the first polarization switching occurs at injection current of 1.2 mA where the y-mode intensity starts lasing with intensity much larger than the x-mode intensity. A second polarization switching is observed at 6.5 mA and the x-mode intensity becomes the larger again. We observe two consecutive polarization switching as we sweep the injection current for VCSEL 2 as well, however, the switching is not as smooth as that for VCSEL 1.

III. EXPERIMENTAL SETUP FOR SYNCHRONIZATION

We use the two VCSELs for our synchronization experiment. Figure 2 shows the experimental setup for chaos synchronization. The two solitary VCSELs (VCSEL 1 and 2) are mutually coupled to each other without an external mirror. The distance between the two VCSELs is set to 0.96 m, corresponding to the one-way coupling delay time of $\tau=3.2$ ns.

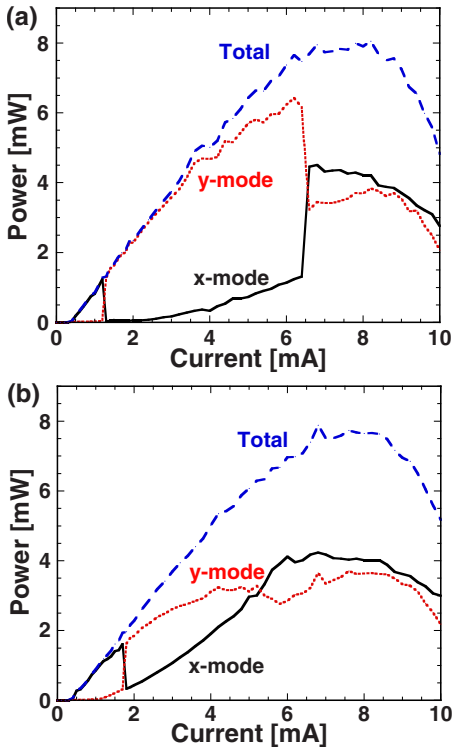

FIG. 1. (Color online) Light power–injection current (*L-I*) characteristics for (a) VCSEL1 and (b) VCSEL2. Solid (black) curve, *x*-mode intensity; dotted (red) curve, *y*-mode intensity; and dashed (blue) curve, total intensity.

A half-wave plate is inserted into the optical path of the two VCSELs to match the polarization direction between the two VCSELs and achieve coherent coupling for both the polarization modes. Each of the two polarization intensities of VCSEL 1 is coupled to that of VCSEL 2. The polarization-resolved temporal dynamics of the two VCSELs are observed by using a digital oscilloscope (Tektronix, TDS7404B, 4 GHz bandwidth, 20 GigaSamples/s) through

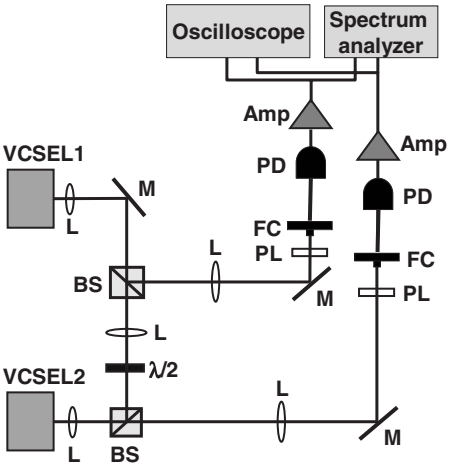

FIG. 2. Experimental setup for chaos synchronization in two mutually coupled VCSELs. Amp, electronic amplifier; BS, beam splitter; FC, fiber collimator; L, lens; λ/2, half-wave plate; M, mirror; PD, photodetector; PL, polarizer.

two photodetectors (New Focus, 1554-B, 12 GHz bandwidth) with electronic amplifiers (New Focus, 1422-LF, 20 GHz bandwidth). The optical wavelengths of the VCSELs are measured by optical spectrum analyzer (Advantest, Q8384). The optical wavelengths of the two VCSELs are controlled by changing the temperature of the VCSELs with a resolution of 0.01 K.

We set the injection currents to 2.50 mA ($6.4I_{th,1}$) and 2.09 mA ($5.6I_{th,2}$) for VCSEL 1 and 2, respectively, above the currents of first polarization switching. The *y*-mode intensity is larger than the *x*-mode intensity at this condition as shown in Fig. 1. We observe the optical spectra of the two VCSELs and confirm that both VCSELs have two-transverse-modes with orthogonal polarizations at these injection currents. However, the fundamental modes are dominant and have much larger power than the first-order transverse mode. The differences in the peak power between the fundamental and first-order modes are 16.7 dB and 9.3 dB for the *y* mode of VCSEL 1 and 2, respectively.

When the wavelengths of the two VCSELs are close enough, wavelength matching (emission at the same wavelength) is achieved under the condition of mutual coupling even though the optical wavelengths of the solitary VCSELs shift toward longer wavelengths. The regions of wavelength detuning for the fundamental modes between the two solitary VCSELs for which this wavelength matching is achieved are 0.058 nm (24 GHz) and 0.067 nm (27 GHz) for the *y*-mode and *x*-mode intensities, respectively.

IV. EXPERIMENTAL RESULTS

A. Temporal wave forms

We observe the polarization-resolved temporal wave forms of the two VCSELs under mutual coupling. We set the wavelengths of 857.988 nm and 857.966 nm for the solitary VCSEL 1 and 2, respectively, and obtain the common optical wavelength of 858.036 nm after the mutual coupling. Figure 3(a) shows temporal wave forms of the *y*-mode intensity for VCSEL 1 and 2. The temporal wave form of VCSEL 2 is shifted with respect to VCSEL 1 by the one-way coupling delay time (τ=3.2 ns) to obtain optimal synchronization. Synchronization of chaos is observed between the *y* mode of VCSEL1 and *y* mode of VCSEL2. The temporal wave forms show in-phase synchronization of chaos. Figure 3(b) shows the correlation plots of the *y*-mode intensities of VCSEL 1 and 2. Good linear correlation is observed and high accuracy of chaos synchronization is achieved. Moreover, the RF spectra of the two VCSELs match well to each other (not shown) and a peak appears at a frequency of 156 MHz, corresponding to the inverse of the round-trip coupling delay time (2τ=6.4 ns) between the two VCSELs.

We also observe the temporal wave forms of the different polarization modes of the two VCSELs. Figure 3(c) shows the temporal wave forms of the *y*-mode intensity of VCSEL 1 and the *x*-mode intensity of VCSEL 2. As in Fig. 3(a), the temporal wave form of VCSEL 2 is shifted by τ with respect to VCSEL 1 in order to obtain optimal synchronization. The temporal wave forms are anticorrelated and antiphase synchronization of chaos is observed. Figure 3(d) shows the

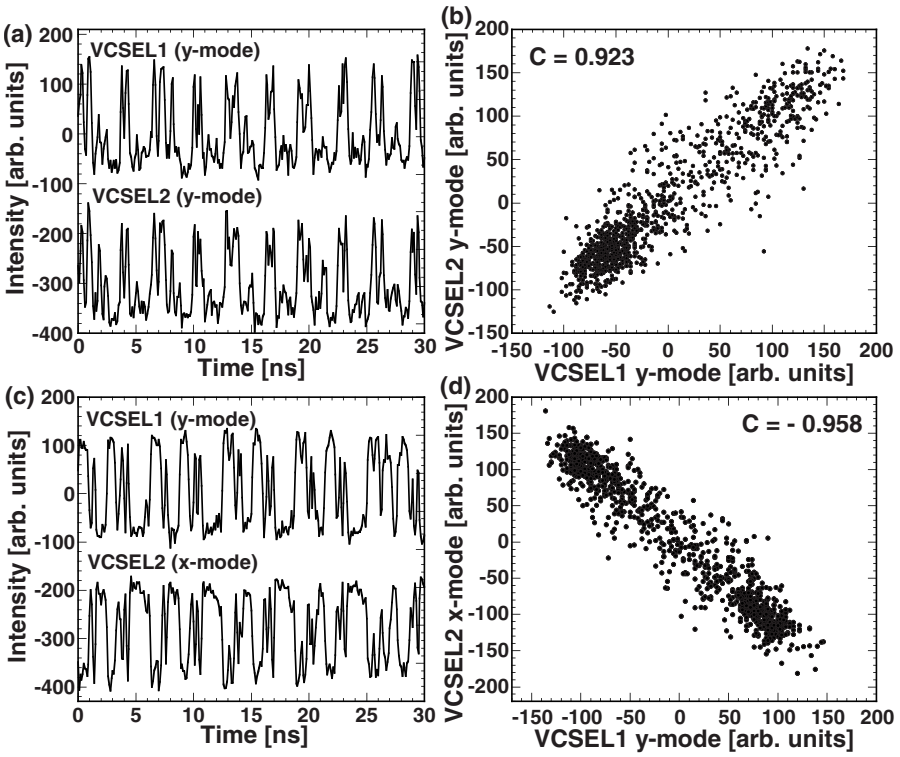

FIG. 3. Experimental result of temporal wave forms and correlation plots for (a),(b) y mode of VCSEL 1 and y mode of VCSEL2, and for (c),(d) y mode of VCSEL 1 and x mode of VCSEL 2. The temporal wave form of VCSEL 2 is shifted with respect to VCSEL 1 by the one-way coupling delay time (τ=3.2 ns) to obtain the optimal synchronization. The cross correlation is (b) 0.923 and (d) −0.958, respectively.

correlation plot between the y mode of VCSEL 1 and the x mode of VCSEL 2. The correlation plot has a negative slope and clearly confirms the antiphase synchronization of chaos. The RF spectra for the two VCSELs look very similar to each other. We speculate that strong antiphase dynamics in the solitary VCSEL is responsible for the antiphase synchronization of chaos.

B. Cross correlation

We quantitatively define the accuracy of synchronization as the cross correlation of two synchronized temporal wave forms normalized by the product of their standard deviations, i.e.,

$$C = \frac{\langle (I_1 - \bar{I}_1)(I_2 - \bar{I}_2) \rangle}{\sigma_1 \sigma_2}, \tag{1}$$

where $I_{1,2}$ are the intensities of the two temporal wave forms of VCSEL 1 and 2, $\bar{I}_{1,2}$ are their mean values, and $\sigma_{1,2}$ are their standard deviations. The angle brackets denote time averaging. The best in-phase and antiphase synchronizations are obtained at cross-correlation coefficients of $C=1$ and -1, respectively.

We calculated the cross-correlation coefficients for the cases of Figs. 3(b) and 3(d) and obtained $C=0.923$ and -0.958, respectively. These values clearly demonstrate the high quality of in-phase and antiphase synchronization of chaos. We thus observe in-phase synchronization of chaos between the same polarization modes and antiphase synchronization of chaos between the orthogonal polarization modes of the two VCSELs.

C. Leader-laggard relationship

As can be seen from Fig. 3, one of the VCSELs leads the other in time by the one-way coupling delay time (τ=3.2 ns). A question arises which VCSEL plays the role of a leader to the other VCSEL (laggard). It is important to investigate the condition that determines the leader-laggard relationship in mutually coupled time-delayed lasers for understanding coupled time-delayed nonlinear systems [12–15].

First we investigate the cross correlation function of the two coupled VCSELs in terms of the time delay T between the two VCSELs as follows:

$$C(T) = \frac{\langle [I_1(t) - \bar{I}_1][I_2(t+T) - \bar{I}_2] \rangle}{\sigma_1 \sigma_2}. \tag{2}$$

Figure 4 shows the cross correlation as a function of the continuous change in the time delay T. Two main peaks appear that correspond to the cross-correlation values shifted by the one-way coupling delay time (τ=3.2 ns) of $T=+\tau$ (called C_+) and $T=-\tau$ (called C_-). Some shorter peaks are also observed, corresponding to the time at $T=\pm(2n+1)\tau$, where n is the integer. The height of the two main peaks changes at different conditions of the optical wavelength detuning for the two solitary VCSELs for Figs. 4(a) and 4(b). The cross correlation at $T=-\tau$ (C_-) becomes larger than that at $T=+\tau$ (C_+) at the positive wavelength detuning of $\Delta\lambda=0.025$ nm [Fig. 4(a)], whereas C_+ is larger than C_- at negative detuning of $\Delta\lambda=-0.033$ nm [Fig. 4(b)], where $\Delta\lambda=\lambda_2-\lambda_1$ is the optical wavelength detuing and λ_i is the optical wavelength of the solitary VCSEL i.

To investigate which VCSEL becomes the leader, we select the two delay times of $\pm\tau$ and shift the temporal wave

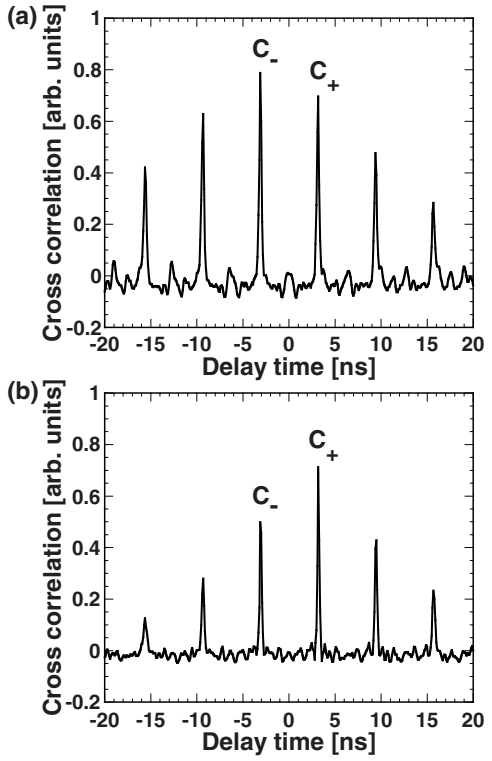

FIG. 4. Experimental result of cross correlation as a function of the continuous change in the time delay T between VCSEL 1 and 2. Two main peaks appear that correspond to the cross-correlation values shifted by the one-way coupling delay time (τ=3.2 ns) of $T=+\tau$ (C_+) and $T=-\tau$ (C_-). (a) $\Delta\lambda=0.025$ nm and (b) $\Delta\lambda=-0.033$ nm, where $\Delta\lambda=\lambda_2-\lambda_1$ is the optical wavelength detuning and λ_i is the optical wavelength of the solitary VCSEL i. The height of the two main peaks (C_+ and C_-) changes at different conditions of the optical wavelength detuning.

form of VCSEL 2 [$I_2(t)$] with respect to VCSEL 1 [$I_1(t)$] by the one-way coupling delay time of τ to both the forward and backward directions in time [i.e., $I_2(t+\tau)$ and $I_2(t-\tau)$]. We calculate the cross-correlation value between $I_1(t)$ and $I_2(t+\tau)$ (C_+), and that between $I_1(t)$ and $I_2(t-\tau)$ (C_-) as follows:

$$C_+ = \frac{\langle [I_1(t)-\bar{I}_1][I_2(t+\tau)-\bar{I}_2]\rangle}{\sigma_1\sigma_2}, \tag{3a}$$

$$C_- = \frac{\langle [I_1(t)-\bar{I}_1][I_2(t-\tau)-\bar{I}_2]\rangle}{\sigma_1\sigma_2}. \tag{3b}$$

We compare C_+ with C_-. When C_+ is higher than C_- we can determine that VCSEL 1 is the leader and VCSEL 2 is the laggard, and vice versa. Figure 5 shows the leader-laggard relationship of the y-mode and x-mode temporal wave forms between VCSEL 1 and 2 when the optical wavelength detuning ($\Delta\lambda=\lambda_2-\lambda_1$) between the solitary VCSEL 1 and 2 is changed. Note that wavelength matching between the two coupled VCSELs occurs due to the mutual coupling in the detuning region shown in Fig. 5. When the solid curve (C_+) is larger than the dotted curve (C_-), VCSEL 1 is the

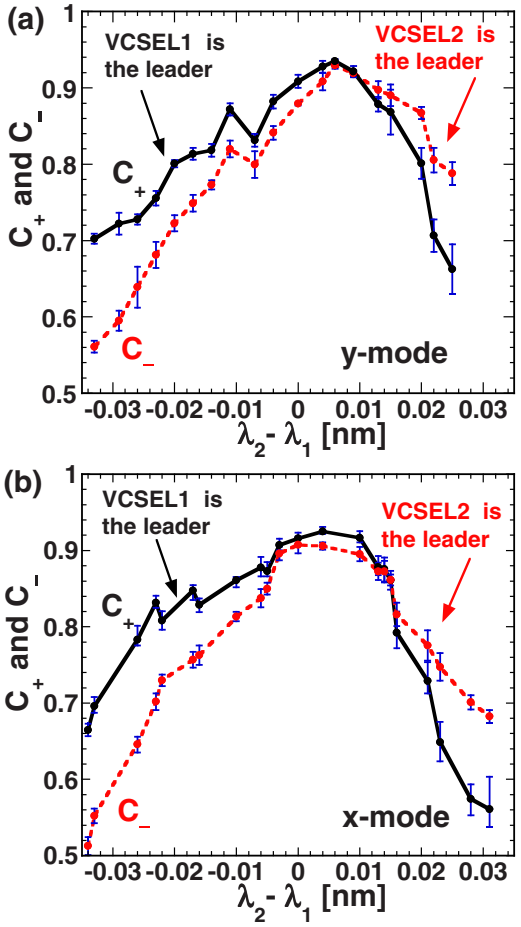

FIG. 5. (Color online) Experimental result of learder-laggard relationship between the synchronized chaotic wave forms of the two VCSELs for (a) y-mode and (b) x-mode intensities when the optical wavelength detuning $\Delta\lambda$ between the solitary VCSEL 1 and 2 is changed, where $\Delta\lambda=\lambda_2-\lambda_1$ and λ_i is the optical wavelength of the solitary VCSEL i. When the solid (black) curve is higher than the dotted (red) curve VCSEL 1 is the leader and VCSEL 2 is the laggard, and vice versa. The VCSEL with longer wavelength becomes the leader.

leader and VCSEL 2 is the laggard, and vice versa. We find that VCSEL 1 becomes the leader at negative $\Delta\lambda$ ($\lambda_2<\lambda_1$) and VCSEL 2 is the leader at positive $\Delta\lambda$ ($\lambda_2>\lambda_1$). Therefore, the VCSEL with longer wavelength becomes the leader.

To reveal the role of injection locking on the behavior of leader-laggard, we put an optical isolator in the optical path between the two VCSELs and look at the optical spectra for the two different directions of optical isolation. We set the condition of the optical wavelength where VCSEL 1 becomes the leader and VCSEL 2 is the laggard, i.e., $\lambda_2-\lambda_1=-0.012$ nm ($\Delta\lambda<0$). Figure 6 shows the optical spectra of two VCSELs under the two different directions of the unidirectional coupling. When the light beam is injected from VCSEL 1 to 2, injection locking is achieved as shown in Fig. 6(a). However, when the coupling is set from VCSEL 2 to 1, injection locking is not achieved. This result indicates that injection locking is achieved only at the negative detuning ($\Delta\lambda<0$) due to the α parameter [16], which can also be observed in edge-emitting semiconductor lasers [17–20].

Therefore, the laser with longer wavelength locks the optical wavelength of the other laser and leads the other laser in time. The leader-laggard relationship is thus determined by the characteristics of injection locking in optically coupled VCSELs.

V. NUMERICAL RESULTS

To confirm our experimental observations we consider a numerical model for mutually coupled VCSELs [21] based on the two-polarization-mode rate-equation model that has been used to explain polarization dynamics of VCSELs with optical feedback [5,6]. The phenomenological rate equations for the two fundamental polarization modes of two mutually coupled VCSELs read as

$$\frac{dE_x^{1,2}}{dt} = \frac{1}{2}(1+j\alpha_x^{1,2})\left(\Gamma_x^{1,2}G_x^{1,2} - \frac{1}{\tau_{px}^{1,2}}\right)E_x^{1,2} + \kappa_x^{2,1}E_x^{2,1}(t-\tau_c^{2,1})\exp(-j\omega_{0x}\tau_c^{2,1}) \pm j\Delta\omega_x E_x^{1,2} + F_x^{1,2}, \tag{4}$$

$$\frac{dE_y^{1,2}}{dt} = \frac{1}{2}(1+j\alpha_y^{1,2})\left(\Gamma_y^{1,2}G_y^{1,2} - \frac{1}{\tau_{py}^{1,2}}\right)E_y^{1,2} + \kappa_y^{2,1}E_y^{2,1}(t-\tau_c^{2,1})\exp(-j\omega_{0y}\tau_c^{2,1}) \pm j\Delta\omega_y E_y^{1,2} + F_y^{1,2}, \tag{5}$$

$$\frac{dN^{1,2}}{dt} = \frac{J^{1,2}}{ed^{1,2}\pi(s^{1,2})^2} - \frac{N^{1,2}}{\tau_e^{1,2}} - G_x^{1,2}|E_x^{1,2}|^2 - G_y^{1,2}|E_y^{1,2}|^2. \tag{6}$$

Here $E_x^{1,2}$ and $E_y^{1,2}$ are the slowly varying x and y LP components of the electric fields in VCSELs 1 and 2 defined in a symmetric reference frame for each polarization, i.e.,

$$\omega_{0x,0y} = (\omega_{x,y}^1 + \omega_{x,y}^2)/2, \tag{7}$$

$$\Delta\omega_{0x,0y} = (\omega_{x,y}^1 - \omega_{x,y}^2)/2, \tag{8}$$

with averaged frequencies $\omega_{0x,0y}$ and frequency detunings $\Delta\omega_{x,y}$. $\alpha_{x,y}^{1,2}$ are the linewidth enhancement factors of the two VCSELs, $\Gamma_{x,y}^{1,2}$ are the confinement factors and $\tau_{px,y}^{1,2}$ are the corresponding photon lifetimes which can also be different for the two orthogonal polarization modes. The mutual coupling is characterized by the coupling-trip delays $\tau_c^{1,2}$ and the coupling strength $\kappa_{x,y}^{1,2}$. The coupling-trip delays $\tau_c^{1,2}$ are given by $\tau_c^{1,2}=2L^{1,2}/c$ with $L^{1,2}$ being the distances for coupling of VCSEL 1 to VCSEL 2 and vice versa, and c is the speed of light.

The coupling strength, i.e., the rate of the injection from one laser into the other, is $\kappa_{x,y}^{1,2}=\eta_{x,y}^{1,2}(1-R^{1,2})/(\tau_{\text{in}}^{1,2}\sqrt{R^{1,2}})$, $R^{1,2}$ being the reflectivity of the front mirror, which we consider the same for the two orthogonal polarizations and for the two VCSELs; $\eta_{x,y}^{1,2}$ are the coupling efficiencies and $\tau_{\text{in}}^{1,2}$ are the photon round-trip times in the cavities, $\tau_{\text{in}\,x,y}^{1,2}=2L_c^{1,2}n_{0x,y}^{1,2}/c$, taken the same for the two polarization modes. In the rate equations for the carrier densities, Eq. (6), $N^{1,2}$ are the carrier densities, $J^{1,2}$ are the injection currents, $d^{1,2}$ are the active region thicknesses, and $s^{1,2}$ are the radii of the apertures and $\tau_e^{1,2}$ are the carrier lifetimes. The material gains for the two polarization modes are given by

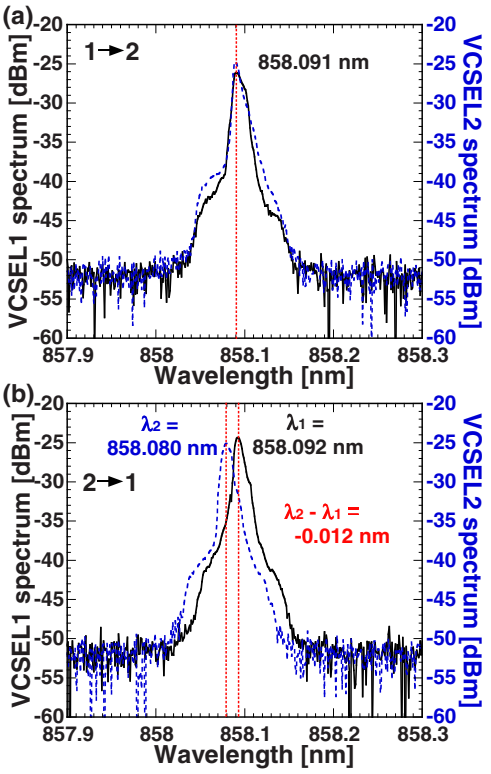

FIG. 6. (Color online) Experimental result of optical spectra of the y-mode intensity of VCSEL 1 and 2 when an optical isolator is inserted in the optical path of the two VCSELS to obtain unidirectional coupling (a) from VCSEL 1 to 2 and (b) from VCSEL 2 to 1. The wavelength of the solitary VCSEL 1 is longer than that of the solitary VCSEL 2. Injection locking is achieved in (a), but not in (b). Solid (black) curve, VCSEL 1; and dotted (blue) curve, VCSEL 2.

$$G_x^{1,2} = v_{gx}^{1,2}g_x^{1,2}(N^{1,2}-N_{tr}^{1,2})(1-\varepsilon_{xx}^{1,2}|E_x^{1,2}|^2-\varepsilon_{xy}^{1,2}|E_y^{1,2}|^2), \tag{9}$$

$$G_y^{1,2} = v_{gy}^{1,2}g_y^{1,2}(N^{1,2}-N_{tr}^{1,2})(1-\varepsilon_{yx}^{1,2}|E_x^{1,2}|^2-\varepsilon_{yy}^{1,2}|E_y^{1,2}|^2), \tag{10}$$

where $v_{gx,y}^{1,2}=c/n_{0x,y}^{1,2}$ are the group velocities, $N_{tr}^{1,2}$ are the carrier densities at transparency which are assumed to be the same for the x- and y-polarized modes and $g_{x,y}^{1,2}$ are the differential gains for the x and y linearly polarized modes in VCSEL 1 and 2. The gain compression is taken into account through $\varepsilon_{x,x}^{1,2}$ and $\varepsilon_{y,y}^{1,2}$—the self-gain saturation coefficients, and $\varepsilon_{x,y}^{1,2}$ and $\varepsilon_{y,x}^{1,2}$—the cross saturation coefficients. The noise due to current injection has been neglected in the rate equation for the carrier density. We consider the following values of the parameters: $\alpha_x^1=\alpha_y^1=\alpha_x^2=\alpha_y^2=3$, $N_{\text{tr}}^1=N_{\text{tr}}^2=4\times10^6\ \mu\text{m}^{-3}$, $\tau_{px}^1=\tau_{py}^1=\tau_{px}^2=\tau_{py}^2=1.3$ ps, $\tau_e^1=\tau_e^2=1$ ns, $n_{0x}^1=n_{0y}^1=n_{0x}^2=n_{0y}^2=3.5$, $L_c^1=L_c^2$

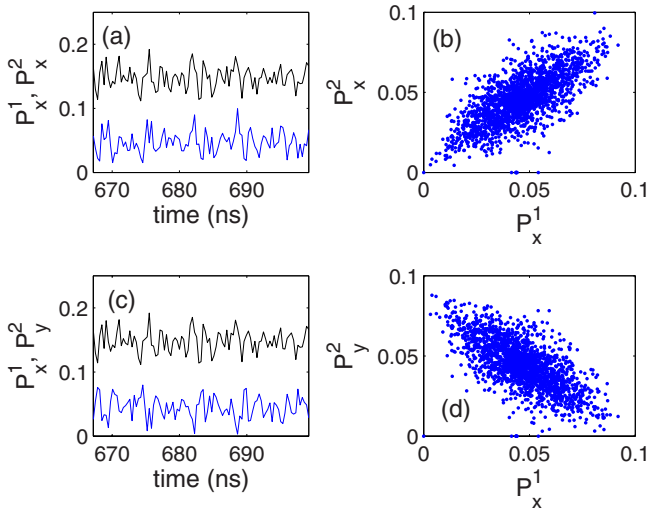

FIG. 7. (Color online) Numerical result of temporal wave forms and correlation plots for (a),(b) x mode of VCSEL 1 and x mode of VCSEL2, and for (c),(d) x mode of VCSEL 1 and y mode of VCSEL 2. The temporal wave form of VCSEL 2 is shifted with respect to VCSEL 1 by the one-way coupling delay time (τ=3.2 ns) to obtain the optimal synchronization.

$=1.97\ \mu$m, $d^1=d^2=0.032\ \mu$m,$s^1=s^2=1.75\ \mu$m, $\Gamma_x^1=\Gamma_y^1=\Gamma_x^2=\Gamma_y^2=0.06$, $R^1=R^2=0.998$, $g_x^1=g_y^1=g_x^2=g_y^2=4\times10^{-8}\ \mu\text{m}^2$, $\varepsilon_{xx}^1=\varepsilon_{yy}^1=\varepsilon_{xx}^2=\varepsilon_{yy}^2=2.5\times10^{-6}\ \mu\text{m}^3$ and $\varepsilon_{xy}^1=\varepsilon_{yx}^1=\varepsilon_{xy}^2=\varepsilon_{yx}^2=5\times10^{-6}\ \mu\text{m}^3$, and $L^1=L^2=0.960$ m.

The VCSELs are biased at $J^{1,2}=1.2$ mA (about 4.5 times the threshold current) and the coupling rates are set at $\kappa_{x,y}^{1,2}=30$ GHz. In Fig. 7 we present the calculated time traces and correlation plots for the polarization resolved intensities of VCSEL 1 and 2 with the VCSEL 2 temporal trace being shifted by the coupling time τ). Similar to the experimental result shown in Fig. 3 synchronization of chaos is observed between the x mode of VCSEL1 and VCSEL2 with the same polarization [see Figs. 7(a) and 7(b)] while the orthogonally polarized modes of the two VCSELs are well anticorrelated and demonstrate antiphase synchronization of chaos [Figs. 7(c) and 7(d)].

The cross-correlation coefficients C_+ and C_- are numerically calculated as a function of the frequency detuning between the two VCSELs, as shown in Fig. 8(a) for the case of symmetric configuration (same injection currents of the two VCSEL) and in Fig. 8(b) for the asymmetric case (the injection current of VCSEL 2 is $J^2=1.05J^1$). Similar to the experimental findings shown in Fig. 5, we observe an exchange of the leader-laggard role depending on the sign of the frequency detuning with a clear tendency for the longer-wavelength VCSEL to be the leader. The switching detuning point of leader-laggard relationship is exactly at $\Delta\lambda=0$ nm for the symmetric situation of Fig. 8(a), but slightly shifted from $\Delta\lambda=0$ nm for the asymmetric situation of Fig. 8(b). This shift is caused by the asymmetry between the two VCSELs. Our numerical simulations confirm that the switching detuning point is shifted from $\Delta\lambda=0$ nm under the condition of an asymmetrical mutual coupling and the shift is similar to the experimentally observed one in Fig. 5.

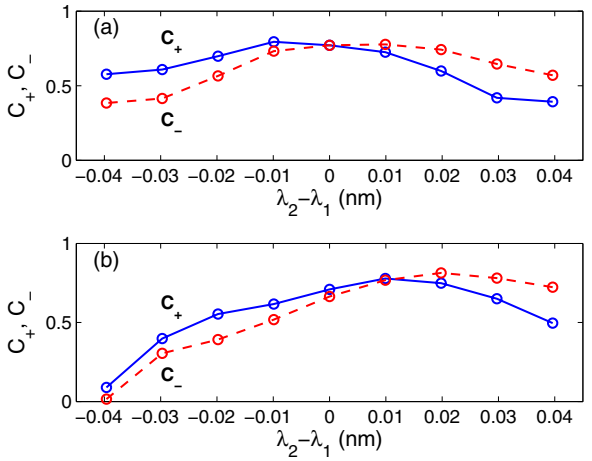

FIG. 8. (Color online) Numerical result of learder-laggard relationship between the synchronized chaotic wave forms of the two VCSELs: (a) symmetric situation ($J^2=J^1$) and (b) asymmetric situation ($J^2=1.05J^1$). When the solid (blue) curve (C_+) is higher than the dashed (red) curve (C_-), VCSEL 1 is the leader and VCSEL 2 is the laggard, and vice versa. The VCSEL with longer wavelength becomes the leader. The switching detuning point of leader-laggard relationship is exactly at $\Delta\lambda=0$ nm for the symmetric situation of Fig. 8(a), but slightly shifted from $\Delta\lambda=0$ nm for the asymmetric situation of Fig. 8(b).

We investigate the role of injection locking on the behavior of leader-laggard. The detuning is set at a negative value $\Delta\lambda<0$ [$\lambda_2-\lambda_1=-0.029$ nm $(-12$ GHz)] for the calculation. Figure 9 shows the numerical results of optical spectra when the coupling is unidirectional. In Figs. 9(a) and 9(c) VCSEL 1 injects light in VCSEL 2 and a sharp single peak is observed in the spectra of both lasers at the frequency of VCSEL 1 indicating that injection locking is established. However, when the isolator is reversed, i.e., VCSEL 2 injects

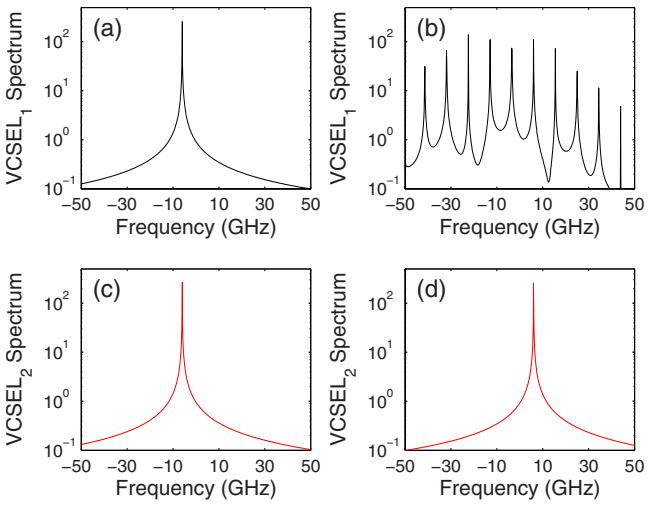

FIG. 9. (Color online) Numerical result of optical spectra of (a),(b) VCSEL 1 and (c),(d) VCSEL 2 when an optical isolator is inserted in the optical path of the two VCSELS for the different directions of optical isolation. (a),(c) Coupling from VCSEL 1 to 2, and (b),(d) coupling from VCSEL 2 to 1. Injection locking is achieved in (a),(c), but not in (b),(d).

light in VCSEL 1, the spectrum of VCSEL 1 shows multiple equally separated peaks indicating that the laser operates in a multiwave mixing regime as shown in Figs. 9(b) and 9(d). These results agree well with our experimental observation shown in Fig. 6 and reveal that there is one-to-one correspondence between the drive laser (identified by optical injection locking) and the leader (identified by the better cross-correlation coefficient at the corresponding delay).

VI. DISCUSSIONS

Our experimental and numerical results confirm that the laser with longer wavelength becomes the leader and the leader-laggard relationship depends on the characteristics of wavelength matching in coupled VCSELs, where injection locking occurs when the wavelength of the injection (drive) laser is longer than that of the injected (response) laser (the negative detuning condition [17–20]). Our interpretation of the physical mechanism of the leader-laggard relationship is the following. When the two VCSELs are mutually coupled to each other, the laser with longer wavelength becomes the drive laser in terms of injection locking, and the optical carrier of the other (response) laser is pulled to that of the drive laser (being also redshifted due to the mutual coupling). The chaotic slow-envelope component of the electrical field of the response laser is also synchronized with that of the drive laser with coupling time delay due to injection locking. Therefore, the drive laser in terms of injection locking becomes the leader of the chaotic oscillation in time. We thus speculate that the dynamics of injection locking in mutually coupled VCSELs determines the leader-laggard relationship.

Our result of the leader-laggard relationship differs from the previous reports in edge-emitting semiconductor lasers [12–14], which indicates that the laser with shorter wavelength (higher energy) becomes the leader. Our observations are confirmed by numerical simulations of a rate equation model suited to describe polarization switching peculiarities of VCSELs [5,6,21]. The leader-laggard relationship may depend on the dynamical regime which is quite different in VCSELs and edge-emitting lasers. In VCSELs we work in the chaotic regime of polarization-dependent dynamics, while the experimental results of edge-emitting lasers were obtained in the low-frequency fluctuation regime [12]. Our experimental and theoretical investigations therefore motivate detailed studies of the leader-laggard relationship and the role of optical injection locking both for edge-emitting lasers and VCSELs.

VII. CONCLUSION

We have experimentally and numerically observed synchronization of chaos in two mutually coupled VCSELs under the condition of wavelength matching. We have observed in-phase synchronization of chaos between the same polarization modes of the two VCSELs and antiphase synchronization of chaos between the orthogonal polarization modes of the two VCSELs. We have investigated leader-laggard relationship between the two VCSELs and found that the laser with longer wavelength becomes the leader. The leader-laggard relationship is strongly related to the characteristics of injection locking in mutually coupled VCSELs.

ACKNOWLEDGMENTS

The authors thank Ingo Fischer, Daan Lenstra, Claudio R. Mirasso, Junji Ohtsubo, Kenju Otsuka, Toni Pérez, and Rajarshi Roy for helpful discussions. A.U. acknowledges support from Support Center for Advanced Telecommunications Technology Research, and Grants-in-Aid for Scientific Research from the Japan Society for the Promotion of Science. K.P. acknowledges support from IAP Program of the Belgian government and GOA, FWO, and OZR of the VUB. M.S. acknowledges the support of Conseil Régional de Lorraine.

[1] M. San Miguel, Q. Feng, and J. V. Moloney, Phys. Rev. A **52**, 1728 (1995).
[2] J. Martín-Regalado, M. San Miguel, N. B. Abraham, and F. Prati, Opt. Lett. **21**, 351 (1996).
[3] C. Masoller and N. B. Abraham, Phys. Rev. A **59**, 3021 (1999).
[4] A. Valle, L. Pesquera, S. I. Turovets, and J. M. Lopez, Opt. Commun. **208**, 173 (2002).
[5] M. Sciamanna, K. Panajotov, H. Thienpont, I. Veretennicoff, P. Mégret, and M. Blondel, Opt. Lett. **28**, 1543 (2003).
[6] K. Panajotov, M. Sciamanna, A. Tabaka, P. Mégret, M. Blondel, G. Giacomelli, F. Marin, H. Thienpont, and I. Veretennicoff, Phys. Rev. A **69**, 011801(R) (2004).
[7] M. Sciamanna and K. Panajotov, Phys. Rev. A **73**, 023811 (2006).
[8] P. S. Spencer, C. R. Mirasso, P. Colet, and K. A. Shore, IEEE J. Quantum Electron. **34**, 1673 (1998).
[9] N. Fujiwara, Y. Takiguchi, and J. Ohtsubo, Opt. Lett. **28**, 1677 (2003).
[10] Y. Hong, M. W. Lee, P. S. Spencer, and K. A. Shore, Opt. Lett. **29**, 1215 (2004).
[11] M. W. Lee, Y. Hong, and K. A. Shore, IEEE Photonics Technol. Lett. **16**, 2392 (2004).
[12] T. Heil, I. Fischer, W. Elsäßer, J. Mulet, and C. R. Mirasso, Phys. Rev. Lett. **86**, 795 (2001).
[13] S. Sivaprakasam, P. S. Spencer, P. Rees, and K. A. Shore, Opt. Lett. **27**, 1250 (2002).
[14] P. Rees, P. S. Spencer, I. Pierce, S. Sivaprakasam, and K. A. Shore, Phys. Rev. A **68**, 033818 (2003).
[15] E. A. Rogers-Dakin, J. García-Ojalvo, D. J. DeShazer, and R. Roy, Phys. Rev. E **73**, 045201(R) (2006).
[16] D. Kuksenkov, S. Feld, C. Wilmsen, H. Temkin, S. Swirhun, and R. Leibenguth, Appl. Phys. Lett. **66**, 277 (1995).
[17] R. Lang, IEEE J. Quantum Electron. **18**, 976 (1982).
[18] T. B. Simpson, J. M. Liu, A. Gavrielides, V. Kovanis, and P. M. Alsing, Appl. Phys. Lett. **64**, 3539 (1994).
[19] S. Wieczorek, B. Krauskopf, and D. Lenstra, Opt. Commun. **172**, 279 (1999).
[20] J. Ohtsubo, *Semiconductor Lasers, Stability, Instability and Chaos* (Springer-Verlag, Berlin, 2006).
[21] K. Panajotov, M. Sciamanna, H. Thienpont, and A. Uchida, Opt. Lett. **33**, 3031 (2008).